A paper for the Third International
Symposium on Science and Engineering
on Cray Supercomputers, Minneapolis,
September 9-11, 1987

CHEMICAL REACTION RATE CALCULATIONS USING A CRAY-2 COMPUTER AND THEIR USE TO TEST APPROXIMATE THEORIES

Kenneth Haug, David W. Schwenke, Yaakov Shima,
and Donald G. Truhlar

Department of Chemistry and Supercomputer Institute,
University of Minnesota, Minneapolis, MN 55455

John Z. H. Zhang, Yici Zhang, Yan Sun, and Donald J. Kouri
Departments of Chemistry and Physics, University of Houston,
Houston, TX 77004

Bruce C. Garrett
Chemical Dynamics Corporation, Upper Marlboro, MD 20772

ABSTRACT

The availability of large-memory vector processing computers opens new possibilities for the efficient solution of the quantum mechanical equations governing chemical reaction probabilities, and we have initiated a program to exploit this opportunity. It is being applied to reactive collisions of an atom with a diatom in either the ground or first excited vibrational state. The method involves solving a set of coupled integral equations equivalent to the Schroedinger equation with scattering boundary conditions by expanding the amplitude density describing the chemical system in a square-integrable ($\mathcal{L}^2$) basis set. This method reduces the computational work involved in the problem to two steps: the numerical evaluation of multidimensional integrals and the solution of large sets of linear equations. Our program is designed to run on a Cray-2 computer, and some of our successful runs have utilized over 128 MW of memory. The results obtained so far are very encouraging, and they have already helped to clarify disagreements between more approximate theoretical results and experimental results.

The reduction of partial differential boundary value problems to quadratures and linear equations may be useful in other fields as well. In quantal collision theory it allows us to perform accurate calculations that in favorable cases may supercede traditional laboratory experiments in accuracy.

The present symposium paper provides a summary of our method and of our first results.

INTRODUCTION

The quantum mechanical calculation of reaction probabilities for chemical collision processes is a subject of great potential usefulness and fundamental interest (Clary[1]), but progress has been slow due to the difficulty of formulating the general problem in a way that is both numerically convenient and rapidly convergent. The recent availability of large-memory vector processing computers, however, has opened the possibility of the efficient solution of the general problem in a new way, and in particular we have decided to explore the possibilities for solving the problem by expansion of the reactive amplitude density in a square-integrable basis defined in coordinates related linearly to Cartesians. The advantages of this approach include ease of integral evaluation, vectorization (Schwenke and Truhlar[2]), and the eventual possibility of using highly optimized basis sets. One way to define basis sets that span the critical intermediate-coupling regions for reactive collisions is to use separate, nonorthogonal sets of direct product bases for each reactant and product's translational, vibrational, and rotational degrees of freedom. In principle, linear combinations of two or more such bases could be overcomplete (Castillejo et al.[3]), but there are several possible ways to couple the various reactant and product arrangements that should converge to unique, well defined answers (Schwenke et al.[4]). We (Haug et al.[5], Zhang et al.[6]) as well as Kuruoglu and Levin[7,8] have found that one of these, the Fock coupling scheme, commonly used in treatments of electron-atom scattering (Burke and Smith[9]) but also applicable to chemical reactions (Miller[10], Schwenke et al.[4]), leads to particularly fast convergence. We have proposed therefore that the equations of the Fock coupling scheme be solved by $\mathcal{L}^2$ expansion of the wave-function or amplitude-density components corresponding to the various arrangements, and we have had good

success with this approach (Haug et al.[5,11], Zhang et al.,[6] and Schwenke et al.[12]). In the present paper we present a description of the Fock-scheme and some results for the chemical reactions of $D + H_2 \rightarrow DH + H$ and $O + H_2 \leftrightarrow OH + H$.

One of the primary motivations for obtaining converged quantal transition probabilities for prototype systems is to use them as benchmarks against which to test more approximate dynamical techniques. In keeping with the goal of treating the quantal dynamics accurately for prototype systems, the present study treats both reactions as electronically adiabatic reactions of distinguishable particles governed by single potential energy surfaces, and the surfaces are assumed to be given by a convenient (though realistic) analytic functions. The accurate results are then used to test variational transition state theory predictions of reaction thresholds and least-action semiclassical calculations of tunneling probabilities, and also to test results based on a coupled states distorted wave approximation.

Further details of the work presented in this symposium paper may be found in Haug et al.[5,11] and Zhang et al.[6,13]

DERIVATION OF COUPLED INTEGRAL EQUATIONS FOR THE AMPLITUDE DENSITY COMPONENTS

In Reference 6 we presented a detailed derivation of the coupled integral equations for the components of the reactive-scattering amplitude-density arrangement components for atom-diatom collisions. Here we summarize that derivation.

The atom-diatom arrangements are labelled by α, where α = 1, 2, 3 denotes A + BC, B + AC, and C + AB, respectively. We scale all coordinates to a reduced mass of

$$\mu = \left[\frac{m_A m_B m_C}{m_A + m_B + m_C}\right]^{1/2} \tag{1}$$

and we denote the mass-scaled Jacobi coordinate in arrangement α by $\vec{r}_\alpha$ for the diatom and $\vec{R}_\alpha$ for relative motion of the atom and the diatom.

Each channel is labelled by a unique collective quantum number $n = \{v_n, j_n, \ell_n\}$, where v_n is a vibrational quantum number

associated with r_α, j_n is a rotational quantum number associated with $\hat{r}_\alpha$, and ℓ_n is an orbital quantum number associated with $\hat{R}_\alpha$. Since each channel is given a unique value of n, it is redundant to also specify the arrangement α, but we do so in most cases anyway because it makes the coupling scheme more clear. The wave function, $\Psi^{\alpha_i n_i}$, is labeled by the initial values α_i and n_i of α and n and is expanded in arrangement components as

$$\Psi^{\alpha_i n_i} = \sum_{\alpha=1}^{3} \Psi_\alpha^{\alpha_i n_i} . \tag{2}$$

In each arrangement we partition the Hamiltonian as

$$H = H_\alpha^A + V_\alpha^D + V_\alpha^C \tag{3}$$

where

$$H_\alpha^A = \lim_{R_\alpha \to \infty} H \tag{4}$$

and

$$V_\alpha^D = \sum_{n=\bar{n}_\alpha}^{\bar{\bar{n}}_\alpha} |\phi_{\alpha n})V_{\alpha n}^D(\phi_{\alpha n}| \tag{5}$$

where $\bar{n}_\alpha = \{1, N_1+1, N_1+N_2+1\}$, $\bar{\bar{n}}_\alpha = \{N_1, N_1+N_2, N_c\}$, and $\phi_{\alpha n}$ is a channel basis function. In Equation (5) we have used the fact that each channel has a unique n so the arrangement index is merely informational. Note that H_α^A is the asymptotic Hamiltonian, including all the kinetic energy terms, V_α^D is the distortion potential, defined for convenience and to accelerate convergence, and V_α^C is a coupling potential without which all rearrangement scattering amplitudes would be zero. The distortion potential is further defined in terms of a single-channel distortion potential $V_{\alpha n}^D$. The channel wavenumber $k_{\alpha v j}$ is defined by

$$k_{\alpha v j}^2 = (2\mu/\hbar^2)(E-\epsilon_{\alpha v j}) \tag{6}$$

where

$$H_\alpha^A \phi_{\alpha n}(\vec{r}_\alpha, \hat{R}_\alpha) = \left[\epsilon_{\alpha v_n j_n} + \frac{\hbar^2 \ell_n(\ell_n+1)}{2\mu R_\alpha^2}\right]\phi_{\alpha n}(\vec{r}_\alpha, \hat{R}_\alpha) \tag{7}$$

The wave function $\Psi^{\alpha_i n_i}$ solves the usual Schroedinger equation

$$(E-H)\Psi^{\alpha_i n_i} = 0 \tag{8}$$

where E is the total energy. Using the partitioning of the Hamiltonian given in Equation (3) allows us to rewrite Equation (8) as

$$(E-H_\alpha^A-V_\alpha^D)\Psi_\alpha^{\alpha_i n_i} = V_\alpha^c \Psi_\alpha^{\alpha_i n_i} + (H-E)\sum_{\alpha' \neq \alpha} \Psi_{\alpha'}^{\alpha_i n_i}. \tag{9}$$

(This is the Fock coupling scheme mentioned in the introduction.) A formal solution to Equation (9) is a coupled system of Lippmann-Schwinger equations given by

$$\Psi_\alpha^{\alpha_i n_i} = \psi^{\alpha_i n_i}\delta_{\alpha\alpha_i} + G_\alpha[V_\alpha^c \Psi_\alpha^{\alpha_i n_i} + (H-E)\sum_{\alpha' \neq \alpha} \Psi_{\alpha'}^{\alpha_i n_i}] \tag{10}$$

where $\psi^{\alpha n}$ solves the distorted wave problem

$$(E - H_\alpha - V_\alpha^D)\psi^{\alpha n} = 0 \tag{11}$$

and G_α is the distorted-wave principal value Green's function defined by

$$G_\alpha = \mathcal{P}(E - H_\alpha - V_\alpha^D)^{-1} \tag{12}$$

where $\mathcal{P}$ denotes a principal value. We define the arrangement coupling matrix as having elements

$$U_{\alpha\alpha'} = \begin{cases} H-E & \alpha \neq \alpha' \\ V_\alpha^C & \alpha = \alpha' \end{cases} \tag{13}$$

which allows us to write Equation (10) as

$$\Psi_\alpha^{\alpha_i n_i} = \psi^{\alpha_i n_i}\delta_{\alpha\alpha_i} + G_\alpha \sum_{\alpha'} U_{\alpha\alpha'}\Psi_{\alpha'}^{\alpha_i n_i}. \tag{14}$$

We now define a Fock-scheme reactive amplitude density $\zeta_\alpha^{\alpha_i n_i}$ to be the operand of the Green's function, i.e.,

$$\zeta_\alpha^{\alpha_i n_i} = \sum_{\alpha'} U_{\alpha\alpha'}\Psi_\alpha^{\alpha_i n_i}. \tag{15}$$

Operating with $\underset{\sim}{U}$ on Equation (14) and using Equation (15) gives

$$\zeta_{\alpha}^{\alpha_i n_i} = U_{\alpha\alpha_i} \psi^{\alpha_i n_i} + \sum_{\alpha'} U_{\alpha\alpha'} G_{\alpha'} \zeta_{\alpha'}^{\alpha_i n_i} \tag{16}$$

and this is the equation we solve by $\mathcal{L}^2$ expansion. That is we now expand the amplitude density as

$$\zeta_{\alpha}^{\alpha_i n_i} = \sum_{nm} a_{\alpha nm}^{\alpha_i n_i} \Phi_{\alpha nm}(\vec{r}_\alpha, \vec{R}_\alpha) \tag{17}$$

where

$$\Phi_{\alpha nm} = R_\alpha^{-1} \phi_{\alpha n}(\vec{r}_\alpha, \hat{R}_\alpha) \lambda_m^{\alpha n}(R_\alpha) \tag{18}$$

and $\lambda_m^{\alpha n}(R_\alpha)$ is a radial translational basis function. In general the radial translational basis functions are nonorthogonal, and their overlap matrix elements are given by

$$\mathcal{O}_{m'm}^{\alpha n} = \int dR_\alpha \lambda_{m'}^{\alpha n}(R_\alpha) \lambda_m^{\alpha n}(R_\alpha). \tag{19}$$

We will also establish a convenient notation for the inverse of this overlap matrix, which is defined as

$$\underset{\sim}{\Delta}^{\alpha n} = (\underset{\sim}{\mathcal{O}}^{\alpha n})^{-1}. \tag{20}$$

Substituting Equation (17) into (16), multiplying by $\Phi_{\alpha n' m'}$, and integrating over the six-dimensional $\vec{r}_\alpha, \vec{R}_\alpha$ space yields the matrix equation

$$\underset{\sim}{a}^{\alpha_i n_i} = \underset{\sim}{b}^{\alpha_i n_i} + \underset{\sim}{C}\, \underset{\sim}{a}^{\alpha_i n_i}. \tag{21}$$

In Equation (21) $\underset{\sim}{a}^{\alpha_i n_i}$ is an unknown vector of expansion coefficients, and the b vector and C matrix have elements given by the integral expressions

$$b_\beta^{\alpha_i n_i} = \sum_{m'} \Delta_{mm'}^{\alpha n} \langle \lambda_{m'}^{\alpha n} \phi_{\alpha n} | R_\alpha^{-1} V_{\alpha_i}^C | \psi^{\alpha_i n_i} \rangle \tag{22}$$

and

$$C_{\beta'\beta} = \sum_{m''} \Delta_{m'm''}^{\alpha' n'} \langle \lambda_{m''}^{\alpha' n'} \phi_{\alpha' n'} | R_{\alpha'}^{-1} (V_\alpha^C G_\alpha - 1) R_\alpha^{-1} | \phi_{\alpha n} \lambda_m^{\alpha n} \rangle \tag{23}$$

where we have used an collective index defined by

$$\beta = (\alpha, n, m); \ \beta' = (\alpha', n', m') \tag{24}$$

and where we have used Equations (11) and (12) to remove the coupling operator $U_{\alpha\alpha'}$.

The transition probabilities that we desire are readily obtained from the reactance matrix (see for example Blatt and

Biedonham,[14] Brandt et al.[15]) which may be written

$$K_{n_f n_i} = \delta_{n_f n_i} {}^{0}K_{n_i}^{\alpha_i} + \mathcal{K}_{n_f n_i} \tag{25}$$

where ${}^{0}K_{n_i}^{\alpha_i}$ is the reactance matrix component due to the distorted wave problem and is obtained in the solution of Equation (11), and $\mathcal{K}_{n_f n_i}$ is the coupling component of the reactance matrix given by

$$\mathcal{K}_{n_f n_i} = -\frac{2\mu}{\hbar^2} \langle \psi^{\alpha_f n_f} | \zeta_{\alpha_f}^{\alpha_i n_i} \rangle \tag{26}$$

or using Equation (17)

$$\mathcal{K}_{n_f n_i} = -\frac{2\mu}{\hbar^2} \sum_{nm} a_{\alpha_f nm}^{\alpha_i n_i} \langle \psi^{\alpha_f n_f} | \Phi_{\alpha_f nm} \rangle . \tag{27}$$

In summary, the desired reaction probabilities are easily obtained from Equations (25) and (27) which requires solving for the $\underset{\sim}{a}^{\alpha_i n_i}$ vector from Equation (21) and doing the integrals in Equations (19), (22), (23), and (27). The integrals involve the coupling potential V_{α}^{C}, the basis functions $\phi_{\alpha n}$ and $\lambda_m^{\alpha n}$, and spherical harmonic functions, and the functions $\psi^{\alpha_i n_i}$ and G_{α} that are readily obtained numerically from the solution of the distorted wave problem of Equation (11). Alternatively the integrals over the radial part of the Green's function in Equation (23) may be generated directly as the solutions of nonhomogeneous differential equations (Schwenke et al.[12]). The computer time requirement is dominated by the solution of the linear equations of Equation (21), and the storage requirements are dominated by the matrices of integrals. (The order of the C matrix is as large as 6063 for the applications presented here.) For the results presented here the $\lambda_m^{\alpha n}$ are distributed gaussian functions (Hamilton and Light[16]) and the $\phi_{\alpha n}$ are expressed in terms of harmonic oscillator functions and spherical harmonic functions.

APPROXIMATE METHODS FOR COMPARISON

We will be comparing our results with two different approximate methods, and they are described very briefly in this section. The comparison itself will be made in the following section.

Variational transition state theory with semiclassical tunneling.

Approximate methods for calculating threshold energies and tunneling probabilities for chemical reactions are of great interest for applications to larger (polyatomic) reactants. The accurate quantum mechanical reaction probabilities obtained on the supercomputer provide an opportunity to test these methods for realistic reactions in three dimensions; (previous work is summarized in Garrett et al.[17]).

First we consider the predictions of quantized variational transition state theory (VTST: Garrett and Truhlar[18,19], Truhlar and Garrett[20]), for selected-vibrational-state threshold energies and of the least-action (LA) semiclassical approximation (Garrett and Truhlar[21]) for tunneling probabilities. In these approximate theories, we begin by defining a reaction path, here taken as the minimum-energy path (MEP), and we compute sets of quantized energy levels for the degrees of freedom orthogonal to this path. For a system with classical motion along the reaction coordinate and a specified value v for the quantum number of the high-frequency stretching vibration, the threshold energy for reaction is given by VTST as the maximum of the state-selected vibrationally adiabatic potential curve defined by (Truhlar and Isaacson[22], Steckler et al.[23])

$$V_a^g(v,s) = V_{MEP}(s) + \epsilon_{str}(v,s) + \epsilon^g_{other}(s) \qquad (28)$$

where s denotes the reaction coordinate (signed distance along the reaction path), $V_{MEP}(s)$ is the Born-Oppenheimer potential along the MEP, $\epsilon_{str}(v,s)$ is the quantized eigenenergy of the vibrational mode that correlates adiabatically to the selected stretch, v is the vibrational quantum number of this stretch, and $\epsilon^g_{other}(s)$ is the ground-state, zero-angular-momentum zero point energy of all the other bound modes. (See Refs. 18, 19.) In the present cases, since the MEP's are collinear, $\epsilon^g_{other}(s)$

is the zero point energy of the doubly degenerate bending mode. The maxima of the curves defined by eq. (28) provide approximate threshold energies in the absence of tunneling, and they provide approximate upper bounds on threshold energies in its presence.

The least-action tunneling approximation is consistent with quantized VTST in that it assumes that the classical turning points for tunneling are given by the locatons at which the total energy E equals the vibrationally adiabatic potential curves of Equation (28). However it also allows for tunneling to occur prior to the system reaching this turning point. In classically allowed regions, the adiabatic approximation is used to define the caustics parallel to the reaction coordinate which define the termini of the tunneling paths. Tunneling is promoted by motion in the vibrational coordinate and, for a given total energy, can begin at any location along a caustic in the asymptotic reactant region up to the turning point in the vibrationally adiabatic potential curve. In the least-action approximation the optimum tunneling path for each pair of termini is chosen from a one-parameter set of parameterized paths by requiring it to be the one that accumulates the least imaginary action along the tunneling path.

The reactions considered here are either thermoneutral or nearly thermoneutral and we treat all tunneling of ground-state reagents as populating only the ground state of products, although this is not necessary (Garrett et al.[24], Kreevoy et al.[25]). For $\rightarrow$ DH + H reaction, vibrational nonadiabaticity is neglected in the approximate calculations because of the mild reaction-path curvature in the vicinity of the dynamical bottleneck for the vibrationally excited reactants, and for the excited-state reaction in this case the full-reaction-path (FRP) adiabaticity approximation (Garrett et al.[26]) is used. For the reactions $O + H_2(v=1) \rightarrow OH + H$ and $OH(v=1) + H \rightarrow O + H_2$ vibrational nonadiabaticity may be important because of the moderate reaction-path curvature, and for these excited-state reactions we use the partial-reaction-path (PRP) adiabaticity approximation (Ref. 26) which assumes that the reaction remains strictly adiabatic up to a location near the first occurrence of an appreciable local maximum of the reaction-path curvature, at which point a sudden nonadiabatic transition is allowed for. For the $O + H_2(v=1) \rightarrow OH + H$ and $OH(v=1) + H \rightarrow O + H_2$ reactions these nonadiabatic transitions occur after the first maxima in the adiabatic potentials (which are different for the forward

and reverse reactions), and for the present applications the location of the sudden transitions are chosen at the local minima of the state-selected v=1 adiabatic barrier. Thus the O + H_2(v=1) reaction is controlled by the highest adiabatic barrier on one side of the region of large reaction-path curvature, and the OH + H reaction is controlled by a (smaller) O-H...H-like barrier on the other side.

Tunneling probabilities for a total energy E and stretching vibrational state v as calculated by the least-action method are denoted $P^{LA}(E,v=0)$ or $P^{LAG}(E)$ for the ground state and $P^{LA}(E,v=1)$ for the excited states. Summing over all states of the bending modes for total angular momentum zero gives the least action approximation to the J=0 cumulative reaction probability $P^{J=0}_{cum}(E)$, (defined by Bowman[27]) to be compared with the quantum mechanical J=0 vibrationally state selected cumulative reaction probability $P^{J=0}_{cum}(E)$, which is given by the sum of all energetically allowed state-to-state reaction probabilities for a given initial vibrational level (i.e., summed over initial rotational quantum number and final rotational and vibrational quantum numbers). In the least-action calculations the contributions from excited states are approximated, analogously to the approximation used in the collinear exact quantum bend-corrected ground-state (CEQB/G) method (Bowman[27]), from the least-action ground-state tunneling probabilities, yielding

$$P^{LA}_{cum}(E,v) = P^{LA}(E,v) + \sum_{i\neq 0} P^{LA}(E - \epsilon_{int}[v,i,s=s^{A}_{*}(v)] + \epsilon_{int}[v,i,s^{A}_{*}(v)],v) \qquad (29)$$

where $s^{A}_{*}(v=0)$ is the location of the maximum of Equation (28), the sum is over excited J=0 bend states [thus i = 0 corresponds in the usual notation (Herzberg[28]) to 0^0, i = 1 to 2^0, i = 2 to 4^0, etc.], and ϵ_{int} is the energy of the bound modes orthogonal to s. The calculational details are as described in Zhang et al.[13].

For D + H_2 and O + H_2 (but not OH + H) the results calculated by Equation (29) are multipled by two because we

consider the sum over the two possible product arrangements (for example, OH + H′ and OH′ + H).

Coupled-states distorted-wave approximation

The accurate quantum results can also be used to test the coupled-states distorted-wave (CSDW) approximation, which has been used by Schatz[29] for the O + H_2 → OH + H reaction. Details of this method are presented elsewhere (Schatz[29], Schatz et al.[30]). In previous applications to the simpler H + H_2 system (Schatz et al.[29]), for which the CSDW results were compared to previous full quantal studies) the CSDW results were found to be nearly equivalent to the exact result at energies where the total reaction probability for each partial wave scattering state is below 10%. Well converged accurate results for the O + H_2 system have not previously been available to make a comparison to the CSDW method. For the CSDW method a direct comparison of state-to-state transition probabilities can be made, although we will also compare some cumulative probabilities in the section below.

COMPARISONS AND DISCUSSION

D + H_2

The H + H_2 reaction and its isotopic analogs have played a central role in the development of gas-phase reaction rate theory (Truhlar and Wyatt[31]), and many aspects of this reaction are well understood. One remaining unresolved question, however has been the quantitative effect of vibrational excitation of H_2 on the reaction rate. There has been a discrepancy between experimental measurements (Kneba et al.[32], Glass and Chaturvedi[33], Rozenshtein et al.[34,35]) which yield a rate constant systematically higher, than several approximate theoretical treatments (Garrett and Truhlar[36], Pollak et al.[37], AbuSalbi et al.[32] and see also Reference 31 of Haug et al.[5]). The threshold energy of the approximate calculations would have to be about 0.04 eV lower for these calculations to agree with these experiments. One recent experimental measurement (Dreier and Wolfrum[39]) is in much better agreement with the approximate

calculations. We have examined this controversy (Haug et al.[5]), where the accurate quantum total reaction probability for D + H_2(v=1,j=0) was compared to the least-action semiclassical results of Garrett and Truhlar[36]. A better way to carry out this comparison, however, is to use the cumulative reaction probabilities discussed above. In this section we compare the vibrationally state selected cumulative reaction probabilities for the threshold region of the D + H_2(v=1) reaction as calculated by the accurate quantal method reviewed above and by the VTST/LA method used by Garrett and Truhlar[36]. These theoretical rate constants are both obtained with the most accurate available potential surface, to be denoted LSTH (Liu[40], Siegbahn and Liu[41], Truhlar and Horowitz[42]). The comparison is made in Figure 1 where very good agreement is seen between the accurate and semiclassical results over the critical threshold region where the cumulative probability is increasing from about 0.01 to 0.1 in value. The solid curve is the semiclassical result of Equation (29), including the factor of two, and the symbols are the quantum mechanical results summed over all states of DH + H' and DH' + H. Extensive convergence tests for the accurate results are presented in References 5 and 6.

The agreement of the accurate results with the semiclassical results and the lower rate constant obtained by the most recent experimental measurement both seem to settle the controversy in favor of the higher threshold energy of the earlier approximate calculations. The agreement of the accurate and semiclassical results also supports the use of the FRP vibrational adiabaticity approximation for this system, as discussed above.

O + H_2

The reaction O + H_2(v) → OH + H has received extensive study in recent years (see for example References 8-34 of Haug et al.[11]) due to its importance in combustion reactions. We will examine this reaction for both v=0 and v=1 by comparison of accurate quantal results to VTST/LA results and for v=0 by comparison to CSDW results. The reverse reaction OH(v=1) + H → O + H_2 will also be examined by comparison of accurate quantal results to VTST/LA results. The v=0 probabilities for the forward and backward reaction differ from each other only by an arrangement

channel multiplicity factor of two, so the v=0 reverse reaction does not provide an independent test and is not included. The potential energy surface used in these calculations is a modified version (Schatz[43]) of the LEPS-type (Sato[44]) surface of Johnson and Winter.[45] Extensive convergence tests of the quantum results have been presented in Zhang et al[13]. The cumulative probability for the reaction $O + H_2(v) \rightarrow OH + H$ for v=0 is presented in Figure 2. The solid curves are the semiclassical results of Equation (29), including the factor of two, and the symbols are the quantum mechanical results summed over all states of OH + H′ and OH′ + H. The accurate and semiclassical methods agree very well for v=0 in the threshold region over the cumulative probability range of 10^{-7} to 10^{-1}. (The wavering about a smooth curve of the semiclassical probabilities above 10^{-1} for v=0 appears to result from the classical turning points being located in a region of high reaction path curvature.)

The cumulative probabilities for the forward reaction $O + H_2(v=1) \rightarrow OH + H$ and the reverse reaction $OH(v=1) + H \rightarrow O + H_2$ are presented in Figure 3. The solid curve is the semiclassical result for the forward reaction, given by Equation (29) including the factor of two, and the dashed curve the semiclassical result for the reverse reaction, given by Equation (29) alone. The accurate results summed over all product states and reactant rotational states are denoted by × for the forward reaction and by ○ for the reverse reaction. The accurate and semiclassical results agree fairly well for the forward reaction but less well for the reverse reaction and this will be discussed below.

The classical barrier height for the surface employed here is 12.5 kcal/mol, at which energy the cumulative probability is about 10^{-3}. Therefore the energy range shown includes energies quite far above the saddle point energy as well as deep into the tunneling region. It is encouraging that the semiclassical method works well in both energy regions.

The energy of the $H_2(v=1,j=0)$ state is 18.0 kcal/mol. As can be seen from Figure 3, the v=1 reaction "turns on" at about 19 kcal/mol of total energy, corresponding to an initial relative translational energy of about 1 kcal/mol, and showing clearly that the vibrational excitation energy is not entirely

available for reaction. The semiquantitative correspondence of the accurate and semiclassical v=1 results in Figure 3 means that the adiabatic approximation employed in the latter are apparently valid in this case, and they provide a simple way to estimate how much of the vibrational energy is available for reaction.

The cumulative probabilities for the reverse reaction, $OH(v=1) + H \rightarrow O + H_2$, are also presented in Figure 3. For the $OH(v=1) + H \rightarrow O + H_2$ case the accurate and semiclassical probabilities for the reverse reaction differ by about one order of magnitude for total energies above about 20 kcal/mol with the semiclassical method overestimating the reaction probability. Since the quantum results for this case appear converged with respect to numerical parameters to the same extent as for the $O + H_2$ reaction discussed in above, one interpretation of the difference of the two sets of v=1 probabilities in Figure 3 is that the reverse v=1 reaction is even more vibrationally adiabatic than assumed in the semiclassical method. The disagreement between the methods can be interpreted as involving the location where the sudden nonadiabatic transition occurs, as discussed above. If the reaction were assumed not to become appreciably nonadiabatic prior to reaching the O---H-H-like adiabatic maximum, which is higher than the O-H---H-like one the VTST-plus-semiclassical-tunneling results would all be smaller. The first VTST adiabatic maximum for OH(v=1) + H is 1.3 kcal/mol lower than the fully adiabatic maximum and the $P_{cum}^{LA}(v=1)$ curve for the reverse reaction is accordingly shifted to the left in Figure 3 (the shift is less than 1.3 kcal/mol because the forward curve involves a factor-of-2 arrangement degeneracy factor). However the accurate quantal results in Figure 3 show a much smaller shift indicating that the higher adiabatic barrier controls the reaction in both directions. Thus the accurate quantal threshold is intermediate between the PRP and FRP predictions, which is similar to what was found for this reaction in the collinear world by Garrett et al.[25]

The accurate quantal results are compared to the CSDW results (Schatz[29]) in Figure 4 for the $O + H_2(v=0, j=0) \rightarrow OH + H$ threshold region, where the probabilities have been summed over all product states. This comparison is shown by the small plot symbols on Figure 4 and the CSDW results are very accurate over the energy range of about 11-18 kcal/mol. Also shown in Figure

4, with the large plot symbols, are the cumulative probabilities for the $O + H_2 \rightarrow OH + H$ reaction for the accurate and CSDW calculations. The cumulative probabilities can also be seen to agree very well.

The remaining rearrangement reaction for this system is the exchange reaction $H + OH' \rightarrow H'O + H$. On the surface used here the classical barrier height for this process is 35.7 kcal/mol above the OH + H potential asymptote, corresponding to a total energy of 38.5 kcal/mol for the zero of energy used here which is the asymptotic $O + H_2$ potential. At the energies we have been examining the reaction probabilities for the exchange reaction are 4 to 10 orders of magnitude smaller than those for the $O + H_2$ reaction and its reverse.

CONCLUDING REMARKS

We have initiated a new program to exploit large-memory vector processing computers to calculate benchmark quantum mechanical reaction probabilities for atom-diatom chemical reactions. We have used these benchmark calculations to test the dynamically approximate variational-transitional-state-theory-with-least-action-tunneling (VTST/LA) and centrifugal sudden distorted wave (CSDW) methods on the $D + H_2(v=1)$, $O + H_2(v=0)$, $O + H_2(v=1)$, and $H + OH(v=1)$ reactions.

A discussion of the memory requirements of our algorithm and the storage strategies we used to implement it is presented elsewhere (Schwenke et al.[46]).

Additional unpublished work has involved the use of multichannel distortion potentials and variational principles to make the method more efficient; initial results are very encouraging (Schwenke et al.[12]). We have checked the variational code for reactive collisions by applying it to the $H + H_2(v=0)$ reaction. We obtain the same results with the variational formulation and a sine basis as we obtained earlier with the method reviewed above and gaussians.

ACKNOWLEDGMENTS

This work was supported in part by the National Science Foundation and the Minnesota Supercomputer Institute.

REFERENCES

1. Clary D. C., ed. (1986), The Theory of Chemical Reaction Dynamics. Reidel D. Dordrecht, Holland.
2. Schwenke D. W. and Truhlar D. G. (1986), Supercomputer Simulations in Chemistry, (Ed. M. Dupuis), p. 165, Springer-Verlag, Berlin.
3. Castillejo L., Percival I. C.,and Seaton M. J. (1960), Proc. Roy.Soc., A254, p. 259.
4. Schwenke D. W., Truhlar D. G., and Kouri D. J. (1987) J. Chem. Phys., 86, p. 2772.
5. Haug K., Schwenke D. W., Shima Y., Truhlar D. G., Zhang J., and Kouri D. J. (1986), J. Phys. Chem. 90, p. 6757.
6. Zhang J., Kouri D. J., Haug K., Schwenke D. W., Shima Y., and Truhlar D. G. J., Chem. Phys. submitted.
7. Kuruoglu Z. C. and Levin F. S. (1982), Phys. Rev. Lett., 48, p. 899.
8. Kuruoglu Z. C. and Levin F. S. (1985), Ann. Phys., 163, p. 149.
9. Burke P. G. and Smith K. (1962), Rev. Mod. Phys., 34, p. 458.
10. Miller W. H. (1969), J. Chem. Phys., 50, p. 407.
11. Haug K., Schwenke D. W., Truhlar D. G., Zhang Y, Zhang J. Z. H., and Kouri D. J., J. Chem. Phys., submitted.
12. Schwenke D. W., Haug K., Truhlar D. W., Sun Y., Zhang J., and Kouri D. J., to be published.
13. Zhang J. Z. H., Zhang Y., Kouri D. J., Garrett B. C., Haug K., Schwenke D. W., and Truhlar D. G. (1987), Faraday Discussion Chem. Soc. 84, submitted.
14. Blatt J. M. and Biedenharn L. C. (1952), Rev. Mod. Phys., 24, p. 258.
15. Brandt M. A., Truhlar D. G., and Smith R. L. (1973), Computer Phys. Comm., 5, p. 456, (1974), 7, p. 177(E).
16. Hamilton I. P. and Light J. C. (1986), J. Chem. Phys., 84, p. 306.
17. Garrett B. C., Truhlar D. W., and Schatz G. C. (1986), J. Amer. Chem. Soc., 108, p. 2876.
18. Garrett, B. C. and Truhlar D. G. (1979), J. Phys. Chem. 83, p. 1079. Errata: (1980) 84, p. 682; (1983) 87, p. 4553.
19. Garrett B. C., Truhlar D. G., Grev R. S., and Magnuson A. W. (1980), J. Phys. Chem., 84, p. 1730. Erratum: (1983) 87, p. 4554.
20. Truhlar D. G. and Garrett B. C. (1980), Accounts Chem. Res., 13, p. 440.
21. Garrett B. C. and Truhlar D. G. (1983), J. Chem. Phys., 79, p. 4931.
22. Truhlar D. G. and Isaacson A. D. (1982), J. Chem. Phys., 77, p. 3516.

23. Steckler R., Truhlar D. G., and Garrett B. C. (1986), J. Chem. Phys., 84, p. 6712.
24. Garrett B. C., Abusalbi N., Kouri D. J., and Truhlar D. G. (1985), J. Chem. Phys., 83, p. 2252.
25. Kreevoy M. M., Ostovic D., Truhlar D. G., and Garrett B. C. (1986), J. Phys. Chem., 90, p. 3766.
26. Garrett B. C., Truhlar D. G., Bowman J. M., and Wagner A. F. (1986), J. Phys. Chem., 90, p. 4305.
27. Bowman K. M. (1985), Advan. Chem. Phys., 61, p. 115.
28. Herzberg G. (1945), Molecular Spectra and Molecular Structure. II. Infrared and Raman Spectra of Polyatomic Molecules. D. Van Nostrand, Princeton, p. 217.
29. Schatz G. C. (1985), J. Chem. Phys., 83, p. 5677 and private communication.
30. Schatz G. C., Hubbard L. M., Dardi P. S., and Miller W. H. (1984), J. Chem. Phys. 81, p. 231.
31. Truhlar D. G. and Wyatt R. E. (1976), Annu. Rev. Phys. Chem., 27, p. 1.
32. Kneba M., Wellhausen U., Wolfrum J. (1979), Ber. Bunsenges, Phys. Chem., 83, p. 940.
33. Glass G. P., Chaturvedi B. K. (1982), J. Chem. Phys., 77, p. 3478.
34. Rozenshtein V. B., Gershenzon Y. M., Ivanov S. D., and Kucheryavii S. I. (1984), Chem. Phys. Lett., 105, p. 423.
35. Rozenshtein V. B., Gershenzon Y. M., Ivanov A. V., Il'in S. D., Kucheryavii S. I., and Umanskii S. Y. (1985), Chem. Phys. Lett., 121, 89.
36. Garrett B. C. and Truhlar D. G. (1985), J. Phys. Chem., 89, p. 204.
37. Pollak E., AbuSalbi N., and Kouri, D. J. (1985), Chem. Phys. Lett., 113, p. 85.
38. AbuSalbi N., Kouri D. J., Baer M., and Pollak E. (1985), J. Chem. Phys., 82, p. 4500.
39. Dreier T. and Wolfram J. (1986), Int. J. Chem. Kinet., 18, p. 919.
40. Liu B. (1973), J. Chem. Phys., 58, p. 1924.
41. Siegbahn P. and Liu B. (1978), J. Chem. Phys. 68, p. 2457.
42. Truhlar D. G. and Horowitz C. J. (1978), J. Chem. Phys. 68, p. 2466; (1979) erratum: J. Chem. Phys., 71, p. 1514.
43. Schatz G. C.(1985), J. Chem. Phys., 83, p. 5677.
44. Sato S. (1955), J. Chem. Phys., 23, p. 592.
45. Johnson B. R. and Winter N. W. (1977), J. Chem. Phys., 66, p. 4116.
46. Schwenke D. W., Haug K., Truhlar D. G., Schweitzer R., Zhang J. Z. H., Zhang Y., Sun Y., and Kouri D. J., Theoret. Chim. Acta, to be published.

FIGURE CAPTIONS

Figure 1. Logarithm to the base 10 of the cumulative reaction probability vs. total energy. The solid curve is the approximate cumulative reaction probability from Equation (29) for $D + H_2(v=1) \rightarrow DH + H$. The × denotes the accurate cumulative reaction probability. The zero of energy is the atom-diatom potential asymptote.

Figure 2. Logarithm to the base 10 of the cumulative reaction probability vs. total energy. The solid curve is the approximate cumulative reaction probability from Equation (29) for the forward reaction $O + H_2(v=0) \rightarrow OH + H$. The × denotes the accurate vibrationally state-selected cumulative reaction probability for this reaction. The zero of energy for Figures 2-4 is the $O + H_2$ potential asymptote.

Figure 3. Logarithm to the base 10 of the cumulative reaction probability vs. total energy. The solid curve is the approximate cumulative reaction probability from Equation (29) for the forward reaction $O + H_2(v=1) \rightarrow OH + H$. The × denotes the accurate vibrationally state-selected cumulative reaction probability for this reaction. The dashed curve is the approximate cumulative reaction probability from Equation (29) for the reverse reaction $H + HO(v=1) \rightarrow O + H_2$. The O denotes the accurate vibrationally state-selected cumulative reaction probability for this reaction. The X and O at 22 kcal/mol are accidently coincident, and the X for 23 kcal/mol is off scale.

Figure 4. Logarithm to the base 10 of the reaction probability vs. total energy. The small × denotes accurate quantal results and small ∘ denotes CSDW for $O + H_2(v=0, j=0) \rightarrow OH + H$. The large × denotes accurate quantal results and large ∘ denotes CSDW results for the cumulative reaction probability for $O + H_2(v=0) \rightarrow OH + H$.

Figure 1

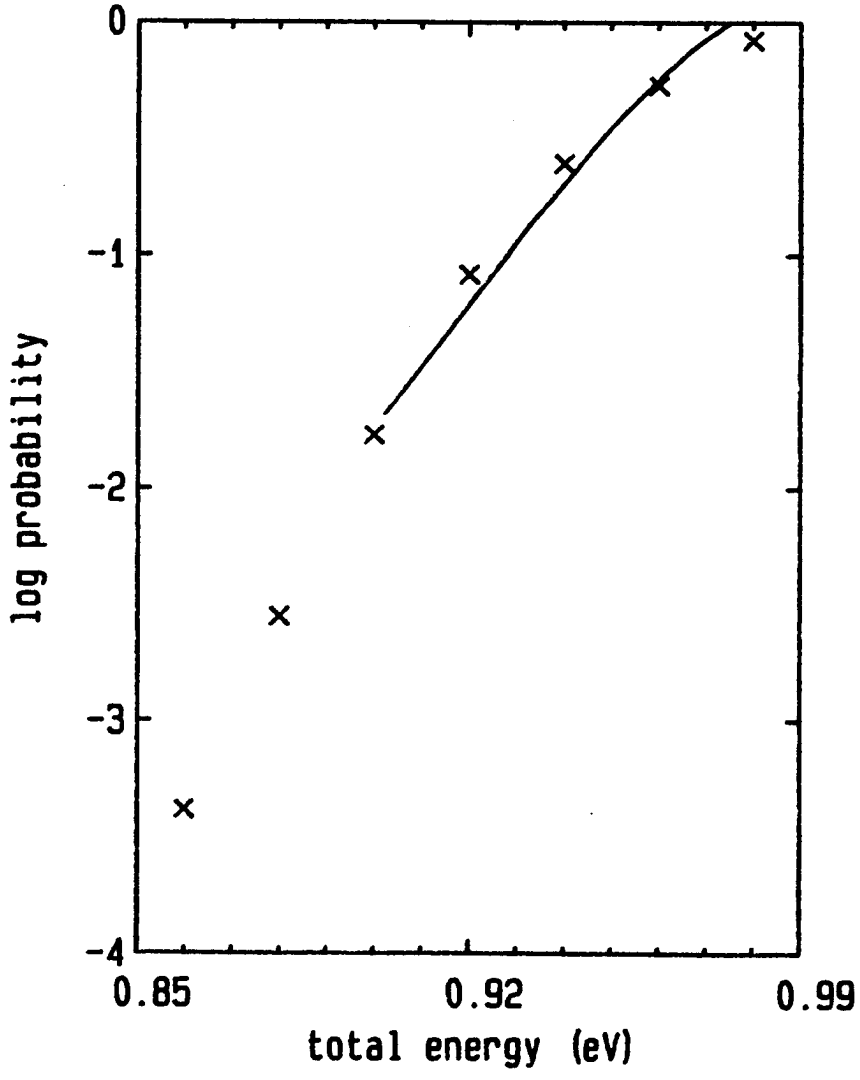

Figure 2

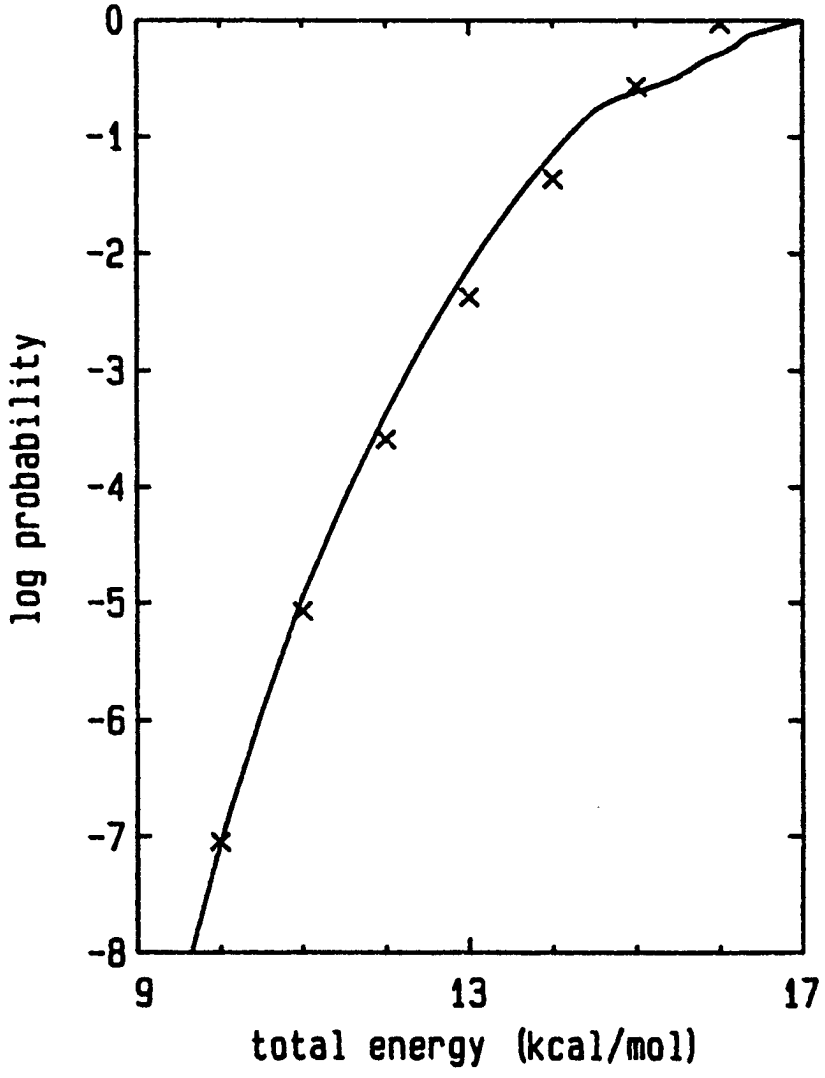

Figure 3

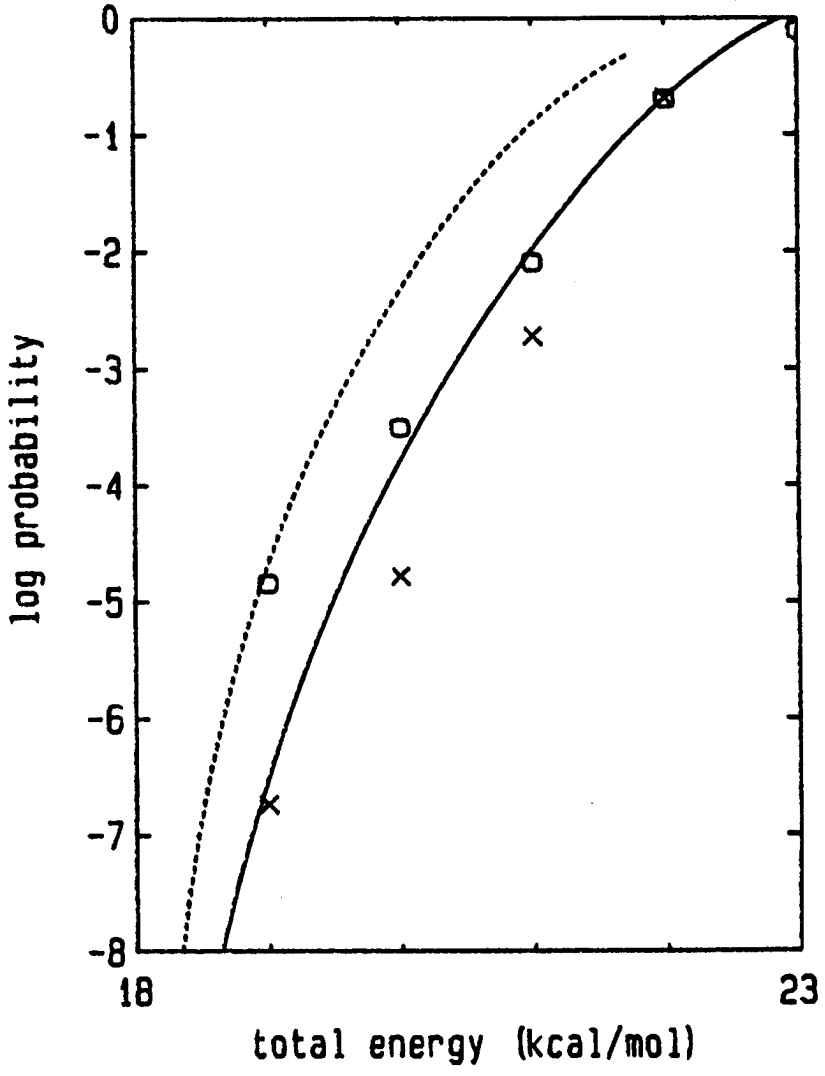

Figure 4